Cement & Concrete Composites 55 (2015) 91–102

Contents lists available at ScienceDirect

Cement & Concrete Composites

journal homepage: www.elsevier.com/locate/cemconcomp

Very early-age reaction kinetics and microstructural development in alkali-activated slag

Berhan S. Gebregziabiher [a], Robert Thomas [a], Sulapha Peethamparan [b,*]

[a] Department of Civil and Environmental Engineering, Clarkson University, 8 Clarkson Avenue, Box 5712, Potsdam, NY 13699, USA
[b] Department of Civil and Environmental Engineering, Clarkson University, 8 Clarkson Avenue, Box 5710, Potsdam, NY 13699, USA

ARTICLE INFO

Article history:
Received 5 December 2013
Received in revised form 31 July 2014
Accepted 4 September 2014
Available online 15 September 2014

Keywords:
Alkali activated slag
Mechanism
Microstructure
BSEM
In-situ isothermal calorimetry
Hydration

ABSTRACT

The early age reaction kinetics and microstructural development in alkali-activated slag binder are discussed. In-situ isothermal calorimetry was used to characterize the reaction progression in sodium hydroxide and sodium silicate-activated slag binders cured at ambient temperature. Microstructure and strength development were monitored to correlate the heat evolution with the property development. In-situ isothermal calorimetric data for sodium hydroxide-activated systems exhibited only one major heat evolution peak with no dormant period. Sodium silicate-activated pastes exhibited multiple peaks and extended dormant periods. Microstructural evolution, monitored using BSE–SEM, showed rapid product formation on the surface of slag grains in sodium hydroxide-activated systems, forming thin reaction shells—the thickness of which was related to the activator concentration—and leading to diffusion controlled hydration at a very early stage. Sodium silicate-activated systems exhibited slow and progressive product formation, predominately nucleated from the solution. These results are supported by electron mapping and electron dispersive X-ray spectroscopy.

1. Introduction

The partial or total replacement of portland cement with supplementary cementitious materials—industrial wastes like fly ashes or ground granulated blast furnace slag (GGBFS)—is a promising solution that addresses the energy and environmental concerns associated with portland cement production without compromising the properties or performance of concrete materials. GGBFS is widely used for portland cement replacement due to its favorable cementitious properties, resulting in cost and emission reductions and performance improvements [1–6]. The use of GGBFS for partial cement replacement has been well studied in the past decades. More recently, a large number of studies have been performed on the use of GGBFS as a sole binding material to further improve the sustainability of concrete production [1–7]. A recent study has estimated that reductions in carbon dioxide equivalent emissions from the use of alkali activated slag in place of portland cement can be as high as 20–45% [8].

GGBFS is a latent hydraulic cementitious material. When used in conjunction with portland cement, the dissolution of GGBFS is promoted as early cement hydration raises the alkalinity of the pore solution. Due to the absence of such a mechanism in the case of total cement replacement, an added alkaline activator is required to promote hydration in latently hydraulic materials like GGBFS and other aluminosilicates [5–7,9–17].

Product formation, microstructural development, and mechanical properties of all cementitious systems are governed by the hydration process [9–16,18–20]. The hydration mechanism of GGBFS in water involves the rapid formation of an aluminosilicate shell on the surface of the slag grains. This shell remains impermeable to water and further reaction will not occur until the shell is broken or dissolved [9,10,18–21]. A highly alkaline environment (pH > 12) is required to dissolve the coating and continue dissolution and subsequent product formation. The mechanism of hydration of ordinary portland cement in water, as many studies have already reported, involves distinct dissolution, induction, acceleration, deceleration and steady state diffusion stages, which are apparent from the heat evolution curve [22–25]. As GGBFS is cementitious, these same stages of hydration are also expected to be observed in the calorimetric curves for alkali activated slag systems. However, the degree of the prevalence of each of these distinct hydration stages and their sensitivity to various parameters, such as the composition of alkali used and environmental conditions, could be very different.

* Corresponding author. Tel.: +1 315 268 4435; fax: +1 315 268 7985.
E-mail addresses: gebregbs@clarkson.edu (B.S. Gebregziabiher), thomasrj@clarkson.edu (R. Thomas), speetham@clarkson.edu (S. Peethamparan).

http://dx.doi.org/10.1016/j.cemconcomp.2014.09.001
0958-9465/

Commonly used activators for GGBFS or fly ash are sodium hydroxide, sodium carbonates, sodium silicates, or other alkalis, which are very corrosive in nature. The critical factors that define these alkalis from an activation perspective are the percentage of sodium oxide (%Na_2O) and the silica modulus (SiO_2/Na_2O) of the solution [9–18,26,27]. Temperature is another factor in hydration which may act as an accelerator during the hydration process [9,10,21,28,29]. The type and composition of the slag may also be a factor in determining the microstructural development and product formation during the activation process [30–34].

This paper seeks to investigate the effect of activator type and dosage on very early age hydration kinetics, microstructural development, and chemical composition of alkali activated GGBFS binder cured at ambient temperature. The reaction kinetics are studied using in-situ isothermal calorimetry which enables the observation of very early age heat evolution, including the one from dissolution stage. The hydration and property development mechanisms are compared among activators, and the poor performance of sodium hydroxide activated GGBFS systems is explained.

2. Materials and experimental methods

2.1. Materials

Grade 100, ASTM C 989 compliant, ground granulated blast furnace slag composed of 36% SiO_2, 10.5% Al_2O_3, 39.8% CaO, 7.93% MgO, 0.27% Na_2O, 2.11% SO_3, 0.16% K_2O, and 0.67% Fe_2O_3 was used as the starting material. The Si/Al ratio, the Blaine surface area and loss on ignition were 3.428, 340 m^2/kg, and 3% respectively. Fig. 1(a) presents the particle size distribution of the slag powder determined using a laser Mastersizer 2000 particle size analyzer. The X-ray diffraction pattern, Fig.1(b), obtained for the slag powder, shows a diffused XRD pattern (a hump) in between 25° and 35° (2θ), which is a typical characteristic of amorphous material.

The alkaline activators used in this study are sodium hydroxide and sodium silicate hydrate solutions. Both are available commercially in the form of reagent grade pellets and liquid solution, respectively. 5, 8, and 12 M sodium hydroxide solutions were prepared by mixing deionized water and sodium hydroxide pellets. Two solutions of sodium silicate were used, with silica moduli (M_s, mass ratio of SiO_2 to Na_2O) of 1.5 and 2.5 and sodium oxide concentration of 2.5% by mass of binder. These were prepared by mixing reagent grade premixed solution with deionized water.

2.2. Experimental methods

2.2.1. Mixing procedure

Binder mixtures were prepared using 5, 8 and 12 M NaOH solutions and 1.5 and 2.5 silica modulus sodium silicate (SS) solutions. All of the pastes were prepared with solution to slag ratio of 0.5 (by mass). Alkaline solutions of the desired concentration were prepared and allowed to cool to room temperature prior to mixture preparation. Mixtures were prepared in the following manner: slag and activator solutions were batched, the solution was added to the mixing bowl, the slag was added within 30 s with the mixer on low speed, mixing continued for another 30 s, the mixer was stopped for 30 s and the bowl was scraped, and the mixture was mixed at high speed for an additional minute.

2.2.2. Compressive strength

50 mm cubic specimens were cast for the determination of compressive strength in accordance with the specifications of ASTM C 39. Specimens were consolidated using a vibrating table and trowel finished. Cast specimens were stored in sealed containers in a moist curing room with humidity in excess of 99% RH and temperature of 23 ± 2 °C. Compressive strength was determined using a hydraulic compression tester at 1, 7, 14, 28, and 56 days.

2.2.3. Reaction kinetics

Typically, hydration kinetics of cementitious systems are studied by ex-situ isothermal conduction calorimetry, in which a mixture of binder and water is prepared outside the calorimeter and is transferred to a small ampoule and then inserted into the calorimeter. The ampoule insertion is typically followed by a stabilization period of up to 45 min, during which thermal equilibrium is reached and no reasonably accurate data can be recorded. As shown in this paper, activated slag exhibit very rapid reactions immediately after mixing, and so ex-situ calorimetry may be inappropriate to evaluate the hydration kinetics of alkali activated systems.

Instead, in-situ calorimetry was performed using a TAM-Air isothermal conduction calorimeter and special in-situ ampoules. The GGBFS and activator solution were stored separately; the former in a glass ampoule, and the latter in an attached syringe. Once the mixing ampoule was inserted into the calorimeter and thermal equilibrium was reached, the activator was injected into the slag and the mixture was mechanically stirred for one minute. The heat evolution was then recorded for the entirety of the hydration process.

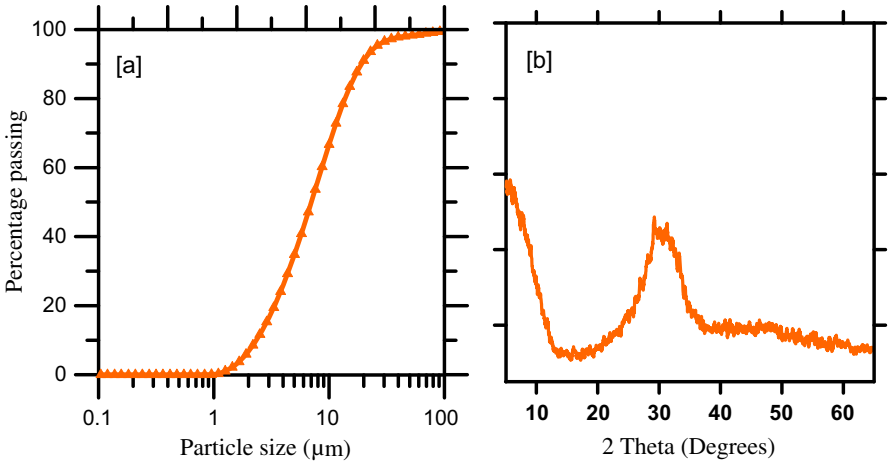

Fig. 1. (a) Particle size distribution of slag powder and (b) X-ray diffraction pattern of GGBFS.

2.2.4. Microstructural and composition

Small cylindrical specimens were cast and cured in the same manner as previously described for analysis of microstructure and product composition. After curing, specimens were sawn into small sections using a slow speed Iso-cut saw, soaked in isopropanol to remove water and quench the hydration reaction, and dried at 50 °C for three days. Specimens were epoxy impregnated and polished to a very smooth surface appropriate for BSE–SEM examination. The specimen preparation protocol used in this study is reported elsewhere in detail [9,35]. Grinding and polishing were performed using 45, 15, 9, 6, 3, 1, and 0.25 μm diamond pastes. Specimens were sputter coated using 60% Gold (Au) and 40% Palladium (Pd) in preparation for microscopy with a JEOL JSM-7400F backscattered scanning electron microscope (SEM. Oxford instruments INCA system was used for energy-dispersive X-ray spectroscopy (EDS) and NORAN microanalysis software was used for quantitative micro analysis.

3. Results

3.1. Compressive strength

The compressive strength of sodium hydroxide (NaOH) and sodium silicate (SS) activated slag paste is presented in Fig. 2. 5 M and 8 M NaOH activated slag showed progressive strength development, approaching the same strength as 12 M activated samples within 28 days. 12 M NaOH activated slag developed 33 MPa strength in one day, weakened slightly thereafter, and did not develop additional strength within 56 days. SS activated slag exhibited steady strength improvement between 3 and 28 days in systems with silica moduli of 1.5 and 2.5; the former developed zero strength after 3 days and 40 MPa after 28 days, and the latter developed 26 and 70 MPa in the same period.

3.2. Hydration kinetics

3.2.1. Portland cement and slag in water

The calorimetric curve for ordinary portland cement (OPC) is known to have five distinctive regions: dissolution, dormancy, acceleration, deceleration, and steady state [22–24,35]. GGBFS hydrates very slowly in water compared to portland cement, which is evident from the calorimetric curves presented in Fig. 3 for 100% OPC, 50% GBFS, and 100% GGBFS pastes with water/binder ratio of 0.5. Slag is amorphous and contains significantly less calcium oxide than portland cement. Unlike portland cement, calcium hydroxide is not a product of slag hydration [3]. Instead, slag hydration results in the formation of silica-rich calcium silicate hydrates (C–S–H), hydrotalcite ($Mg_6Al_2(CO_3)(OH)_{16}{\cdot}4(H_2O)$), and traces of ettringite $Ca_6Al_2(SO_4)_3(OH)_{12}{\cdot}26H_2O$ or monosulfate ($Ca_4Al_2O_6(SO_4){\cdot}14H_2O$) [11,30,36]. However, the reaction is slow enough that no measurable heat is evolved over a period of 48 h, indicating the absence of the formation of reaction products.

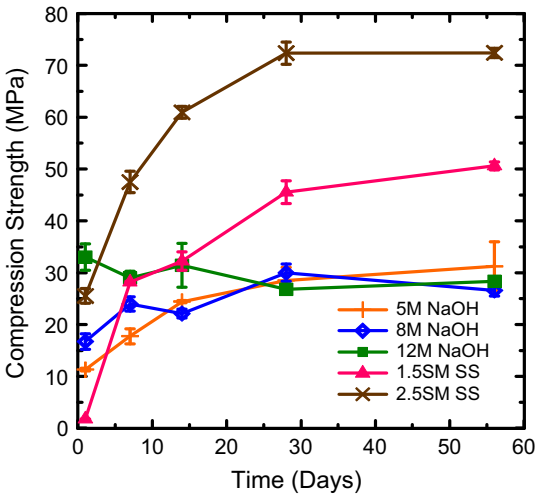

Fig. 2. Compressive strength development in slag activated with NaOH (5, 8 and 12 M) and SS (silica modulus of 1.5 and 2.5) solutions.

The specimen prepared with 100% GGBFS showed no heat evolution over the first 4 days of hydration. When slag is used for partial cement replacement, the cement hydrates first and raises the pH of the pore solution sufficiently to allow dissolution of the impermeable shell formed on the surface of slag particles. This is marked by significant heat evolution, seen in the calorimetric curve of the specimen containing 50% GBFS. The presence of portland cement initiates the hydration reaction, leading to dissociation of ions into the pore solution followed by formation of hydration products in the system. This process increases the alkalinity of the pore solution, thereby activating the slag.

3.2.2. Sodium hydroxide activated slag

Calorimetric curves for 5, 8, and 12 M NaOH activated slag at 25 °C are presented in Fig. 4; Fig. 4(a) shows the heat evolution over the first 24 h, Fig. 4(b) shows the heat evolution in the first 2 h, and Fig. 4(c) shows the cumulative heat evolved in the first 24 h. The distinctive processes identified in a normal cement hydration curve such as dissolution/wetting, acceleration and deceleration stages were observed in 5 M and 8 M NaOH-activated systems, but the duration of each stage was very short compared to portland cement hydration (Fig. 3). The dissolution peak in NaOH activated slag occurred within the first 15 min of hydration, and the acceleration peak occurred around 30 and 45 min of hydration for 5 M and 8 M systems, respectively. The deceleration period for both ended in about six hours, at which point both entered steady state. No noticeable induction period was observed. Only one major peak was observed in the calorimetric data for 12 M NaOH activated slag, which occurred immediately after adding the activator. No distinct dissolution, induction, or acceleration stages were noted and the deceleration stage was relatively long, lasting approximately 18 h. The reaction reached a steady state after 18 h, and no further peaks were recorded. The magnitude of the initial peak (Fig. 4(b)) was influenced by the molarity of the sodium hydroxide activator, with the heat flow increasing with molarity.

The cumulative heat flow curves for NaOH activated slag (Fig. 4(c)) indicate more heat evolved–and therefore a higher degree of hydration–at 12 M between 10 and 60 h. However, the curves for all three activator concentrations converge to the same degree of hydration near the end of the third day. Thereafter, 5 M and 8 M systems tended to show a higher degree of hydration. This implies an inverse relationship between the molarity of the NaOH activator and the total heat evolution.

3.2.3. Sodium silicate activated slag

Calorimetric curves for SS activated slag are presented in Fig. 5; Fig. 5(a) shows the heat evolution over the first 72 h, Fig. 5(b) shows the heat evolution in the first 2 h, and Fig. 5(c) shows the cumulative heat evolved in the first 150 h. Both silica moduli resulted in high exothermic peaks immediately after mixing, followed by a very long induction period. With silica modulus of 1.5, induction period ended only after 35 h and was followed by 8–10 h acceleration and deceleration periods, reaching steady state diffusion-controlled stage after about 70 h. In contrast, at silica modulus of 2.5, two dormant periods and three exothermic peaks were observed. The first exothermic peak occurred immediately after mixing, followed by a 15-h induction period, another small

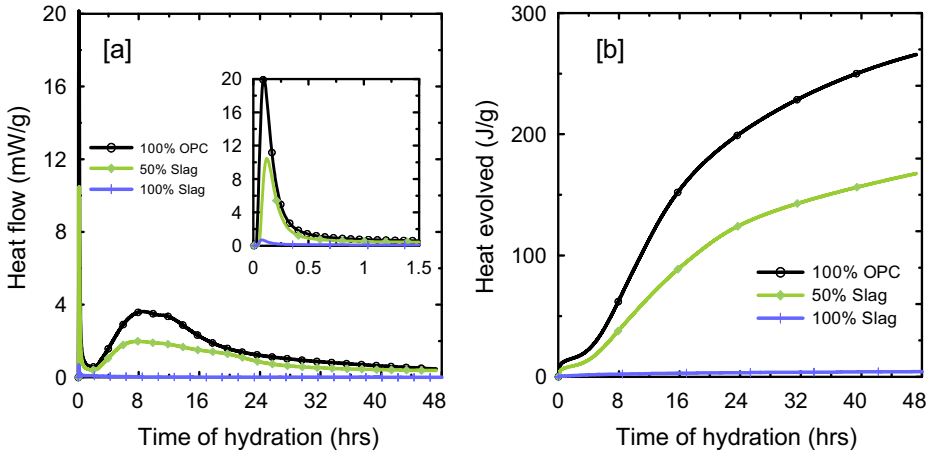

Fig. 3. (a) Hydration curve of and (b) heat evolved from 100% OPC paste, 50/50 OPC/slag paste and 100% slag (sole slag) paste, each at 25 °C.

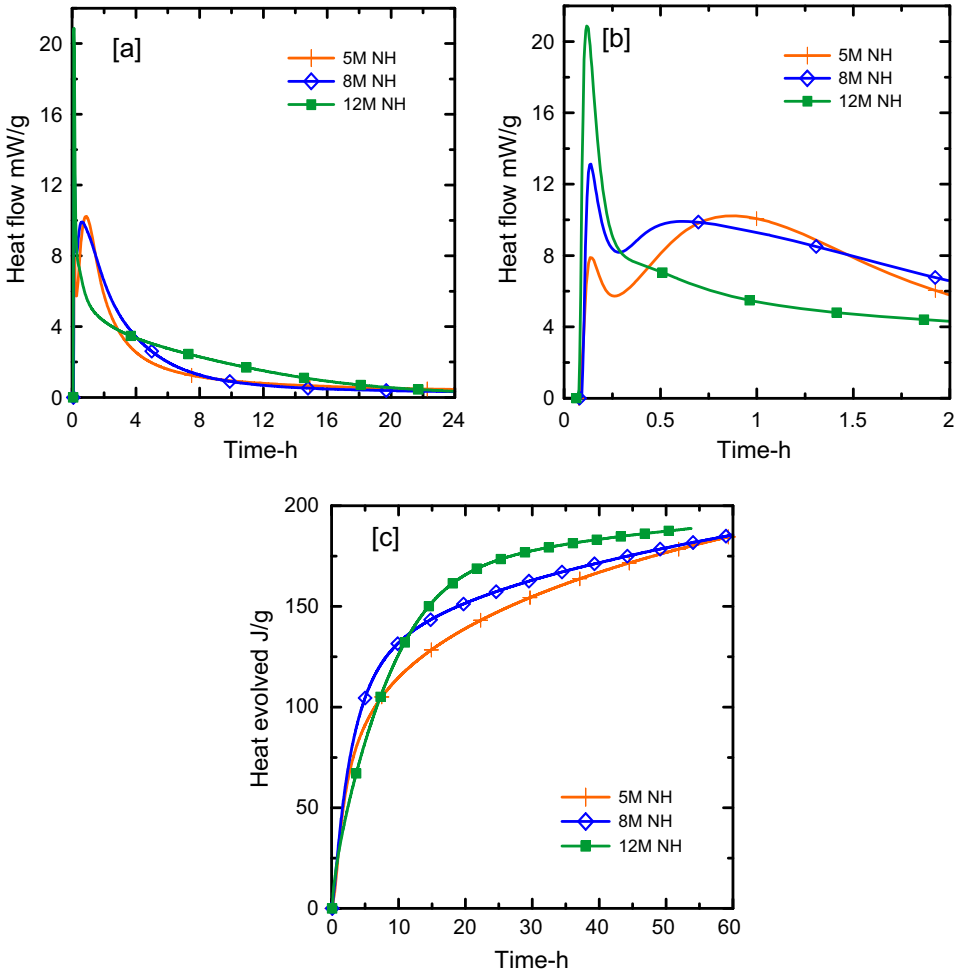

Fig. 4. (a), (b) Hydration curve of and (c) heat evolved from 5 M, 8 M and 12 M NaOH-activated slag at 25 °C.

exothermic peak, a 10-h dormant period, and a broader exothermic peak. Since the activators were prepared with constant concentration of Na_2O and varied concentration of SiO_2, these data imply that SiO_2 concentration has a strong effect on the reaction kinetics and the degree of hydration in activated slag systems.

The cumulative heat flow curves for SS activated slag (Fig. 5(c)) indicate a higher degree of hydration with increased silica modulus beginning around 48 h. During the first 20 h, the opposite is true. This is likely due to the difference in alkalinity; the measured pH of 1.5 and 2.5 silica modulus activator solutions were 12.97 and 11.8, respectively (as measured using Denver Instruments UB-5 high alkalinity pH meter). A higher proportion of sodium is present when the silica modulus is reduced, resulting in increased alkalinity. As seen in NaOH activated systems, increased alkalinity

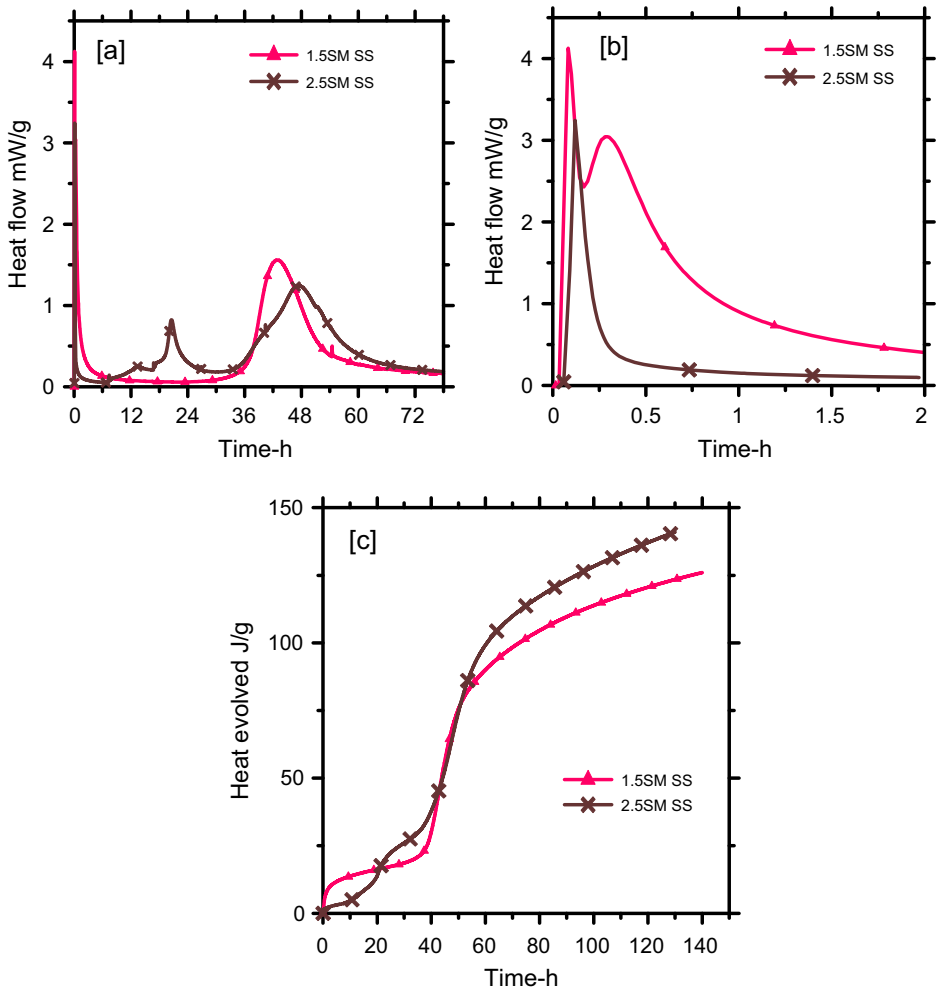

Fig. 5. (a), (b) Hydration curve of and (c) heat evolved from 2.5% Na_2O with 1.5 and 2.5 SM [SiO_2/Na_2O] at 25 °C.

tends to promote faster reaction progression during early reaction stages. However, after the initial stages of hydration, higher silica content and lower pH tend to favor the dissociation of calcium [20,37]. As a result, the higher silica modulus results in more overall heat evolution and product formation.

Comparing the cumulative heat evolution of NaOH and SS activated slag (Figs. 4(c) and 5(c)), it is evident that NaOH activated systems exhibit higher cumulative heat of reaction. However, SS activated pastes exhibited higher compressive strength. This indicates that strength development of alkali activated slag depends not only on the degree of hydration, but also on the microstructural development and phase compositions.

3.3. Microstructural development

The microstructural development in NaOH and SS activated slag was studied by analyzing over 200 SEM micrographs taken using backscattered electron microscopy for each mixture at various curing periods. For the sake of brevity, only representative micrographs are included in the paper.

3.3.1. Sodium hydroxide activated slag

NaOH activated slag mixtures exhibited rapid product formation around individual slag grains as well as in the matrix of the system immediately after combining the slag and activator. It appears that the highly alkaline environment provided by the NaOH activator resulted in immediate dissolution of the slag and subsequent product formation. These rapid microstructural developments are displayed in Fig. 6, which show the microstructure of 8 M and 12 M pastes after 3 and 6 h of hydration. The microstructure was fully developed within 3 h, with two main distinguishable phases: unreacted slag grains and activated gel products (outer products—OP) in the matrix (hereafter referred as the outer product-OP). After six hours, the formation of a reaction ring around the slag grains (inner product—IP) was evident, but no other significant differences were observed.

The thin inner product shell, as shown in Fig. 7, forms around the grains during the initial reaction period, limiting the degree of dissolution of the slag grain. Further reaction progression is therefore limited by the diffusion rate of the activator solution into the slag grain. As such, the degree of diffusion through the inner product shell becomes a significant factor in the microstructural development at early age since the formation of products is dependent on the availability of ions in the pore solution and their ability to penetrate the inner product shell [11,21,38]. It is apparent that microstructural development in NaOH activated slag can be compared with that of the shrinking core model and ground mass models generally used for portland cement hydration. The shrinking core model represents the formation of inner products due to the diffusion of pore solution into the slag grains, thereby reducing the size of the unreacted slag grains [11,24,36]. The groundmass model represents the nucleation of the new products from the

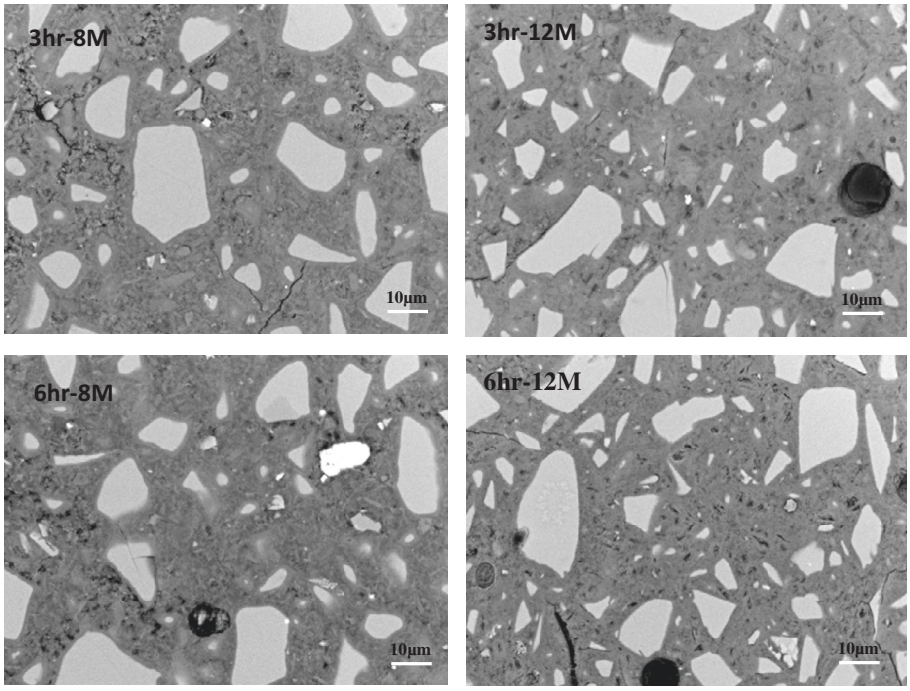

Fig. 6. 8 M and 12 M-NaOH activated slag after 3 h and 6 h of hydration.

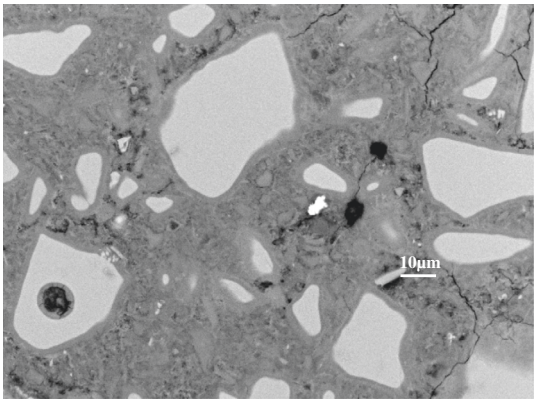

Fig. 7. 8 M NaOH activated slag after 6 h of hydration.

dissociated ions in the solution [24]. The evolution of the microstructure for 8 M NaOH-activated slag samples showing the progressive shrinking of the unreacted slag grains and the densification of the ground mass of the matrix with curing duration is presented in Fig. 8.

The rate of product formation around slag grains varies with the molarity of the NaOH activator, as indicated by the thickness of the inner product shell after 28 days shown in Fig. 9. The inner product shell becomes relatively thin with increased molarity, although it appears that the ionic diffusivity is reduced by the increased density of the inner product shell at high molarity. As a result of this reduced diffusion, large slag grains remain unreacted, as seen in Fig. 9(c). On the other hand, noticeable shrinking cores are observable at low molarity.

3.3.2. Sodium silicate activated slag

Microstructural development in SS activated slag is quite different from that observed in NaOH activated slag, as shown in Fig. 10. In the former, microstructural development is very slow during the early reaction stages; progressive product formation and microstructural development with silica modulus of 1.5 can be seen at 1, 7, and 28 days in Fig. 10(a)–(c). It is apparent that sodium silicate activators promote the dissolution of slag for a considerable amount of time, and that product formation occurs by nucleation from the solution. No visible inner product ring formation was observed, but a dense matrix was developed in the ground mass.

Despite significant differences in hydration kinetics, the microstructural development in sodium silicate activated slag with silica modulus of 2.5 was very similar to that with silica modulus of 1.5. A comparison of both systems after 24 h is presented in Fig. 11. Slightly more product formation is observed with higher silica modulus (Fig. 11(b)). Similarly, Fig. 12 shows the microstructure at both silica moduli after 28 days of hydration. Neither silica modulus resulted in the formation of an inner product ring as observed in NaOH activated slag. The main visible course of product formation with both silica moduli was through precipitation of ions from the solution, commonly referred to as 'through solution' precipitation [38].

3.4. Microstructural composition

Energy dispersive X-ray spectroscopy (EDS) was used to determine the quantitative elemental composition of the aforementioned microstructural phases in order to compare the chemical composition of these components among different activators and concentrations. Fig. 13 shows representative locations of the different phases that were taken for the elemental analysis. results of the analysis for NaOH and SS activated pastes are presented here.

3.4.1. Sodium hydroxide activated slag

The EDS spectra collected from NaOH activated slag are presented in Fig. 14. Locations 1, 2 and 3 refer to unreacted slag (UG), outer product (OP) and inner product (IP), respectively. Sublocations a, b, and c refer to 5, 8 and 12 M activators, respectively. The composition of unreacted slag grains was nearly identical for all molarities with no significant sodium content. Inner and outer

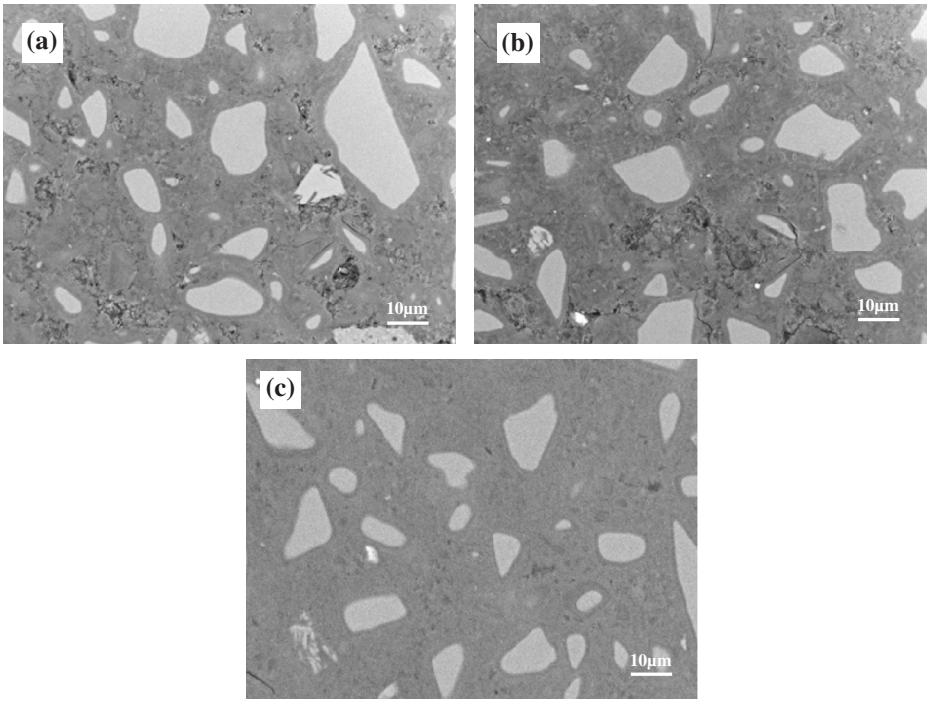

Fig. 8. 8 M NaOH activated slag after (a) 24 h (b) 7 days and (c) 28 days of hydration.

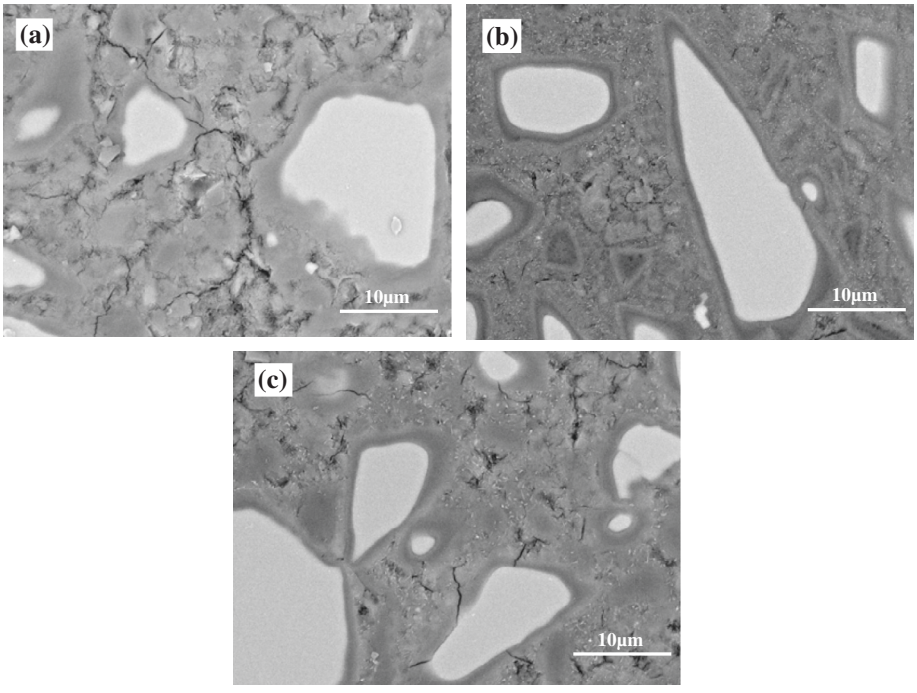

Fig. 9. (a) 5 M (b) 8 M and (c) 12 M NaOH-activated slag after 28 days of hydration.

product compositions were also similar for all molarities, with higher sodium content in the outer product; this difference was magnified as activator molarity increased. The main product components were silicon (Si) and calcium (Ca) with lesser amounts of sodium (Na), magnesium (Mg), and aluminum (Al).

A summary of the elemental atomic ratios within the inner product of NaOH activated slag is provided in Table 1. The relative concentrations of calcium and sodium to silicon (Ca/Si and Na/Si) increase with activator molarity. Higher Ca/Si and Na/Si is indicative of the formation of denser, calcium and sodium-rich products on the surface of slag grains with increased activator molarity. The abundance of aluminum in the products was not influenced significantly by the concentration of the NaOH solution activator.

To further analyze the elemental composition, electron mapping under energy dispersive spectroscopy (EDS) was performed on 8 M NaOH activated slag after 28 days of hydration. The resulting electron maps, presented in Fig. 15, show the diffusion and distribution of the alkali elements into the slag grains and the

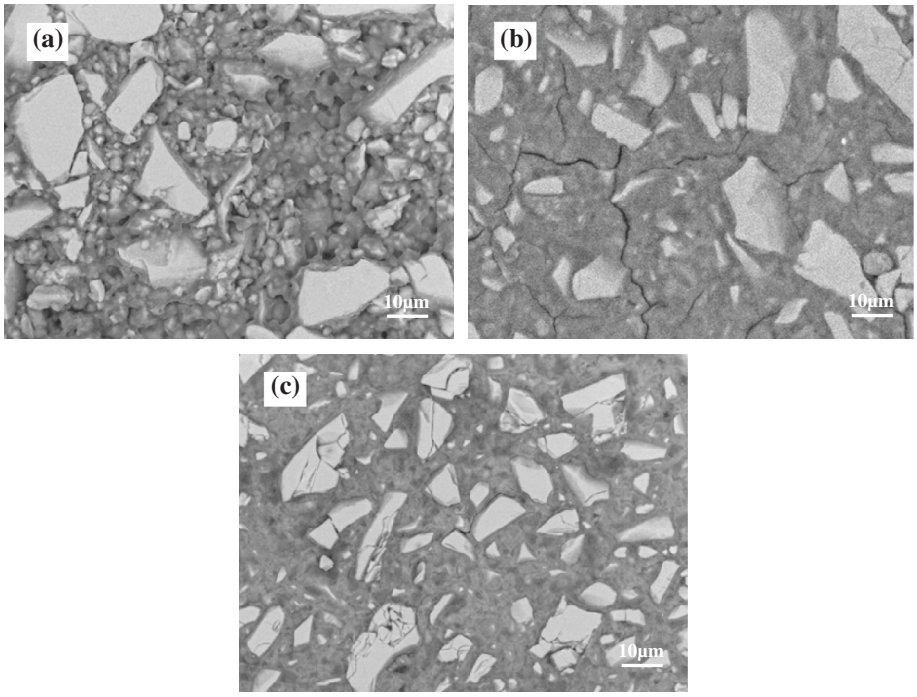

Fig. 10. Microstructure development in 1.5 silica modulus activated slag after (a) 24 h (b) 7 days and (c) 28 days of hydration.

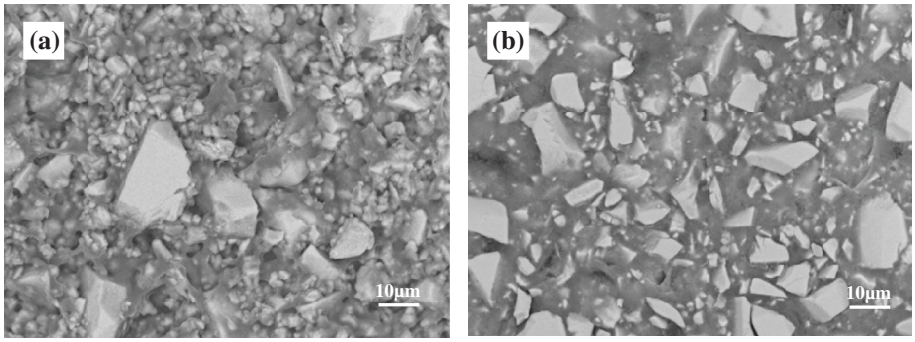

Fig. 11. Microstructure of (a) 1.5 silica modulus and (b) 2.5 silica modulus SS activated slag after 24 h of hydration.

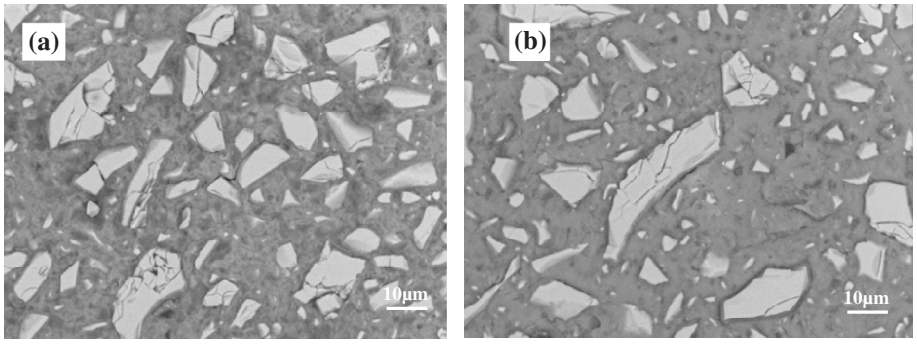

Fig. 12. Microstructure of (a) 1.5 silica modulus and (b) 2.5 silica modulus SS activated slag after 28 days of hydration.

dissociation of the slag grains into the pore solution. The concentration of sodium, provided by the activator and originally present only in the pore solution, is a good indicator of diffusion of this ion through the shell. Higher presence of sodium in the matrix and lower presence inside the grain means lower diffusion through the shell. Traces of calcium from the slag grains can be seen scattered in the matrix showing the initial dissolution of the slag particles from the grains.

3.4.2. Sodium silicate activated slag

The chemical composition of the ground mass gel product in SS activated slag paste was similar to that of NaOH activated slag but

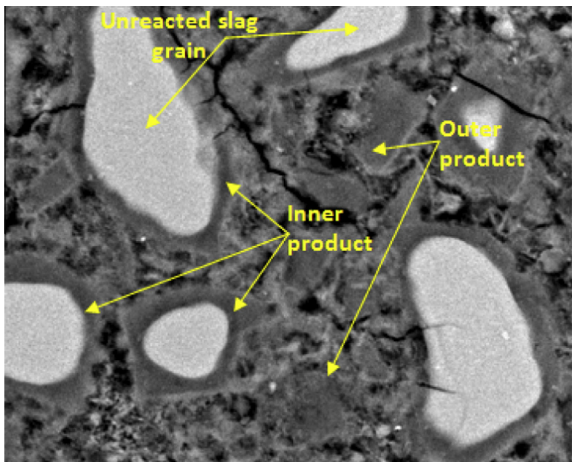

Fig. 13. Representative image of the different phases of hydration products.

with relatively lower concentrations of Na and Si. This can be seen in Fig. 16. The concentration of sodium in SS activators was lower than that of NaOH activators. Further, the concentration of silicon increased with silica modulus, as expected. The sodium content remained about the same regardless of silica modulus, which stands to reason as the sodium oxide concentration was the same for both activator solutions. No other significant difference was observed in the product composition of SS activated slag pastes.

Electron maps for SS activated slag with silica modulus of 1.5 after 28 days of hydration are presented in Fig. 17. The abundance of calcium within the matrix is indicative of adequate dissociation of the slag grains into the pore solution, more so than in the outer product of NaOH activated pastes. Similarly, the distribution of sodium has a pronounced difference between the two activators. Although the sodium content of SS activators was lower than NaOH activators, the diffusion of sodium into the slag grains was relatively higher in SS activated slag. This indicates that SS activators have ample diffusion of pore solution into slag grains relative to NaOH activators.

Table 1
Comparison of elemental ratios of slag product around unreacted grains activated by 5 M, 8 M and 12 M NaOH solutions.

	Ca/Si	Al/Si	Na/Si
5 M	1.12	0.37	0.05
8 M	1.16	0.31	0.14
12 M	1.39	0.31	0.65

4. Discussion

The results presented here show that the hydration kinetics of alkali activated slag are very different from those of pure portland cement and blended GGBFS and portland cement. NaOH activated slag reacted spontaneously with no induction period, while SS activated slag tended to exhibit long induction periods with two stages of product formation. The calorimetric curves for NaOH-activated systems showed much shorter induction periods of a few minutes, which may be a limiting factor for using these binders in real applications because of their very short setting times [16]. Proper delaying of the setting time will be a challenge for NaOH activated slag binders, and the authors' experience shows that most commercially available retarders for portland cement binders are not effective in activated slag systems. On the other hand, the induction period in sodium silicate activated slag (20–45 h) is very long, which may also limit the use of these binders unless appropriate

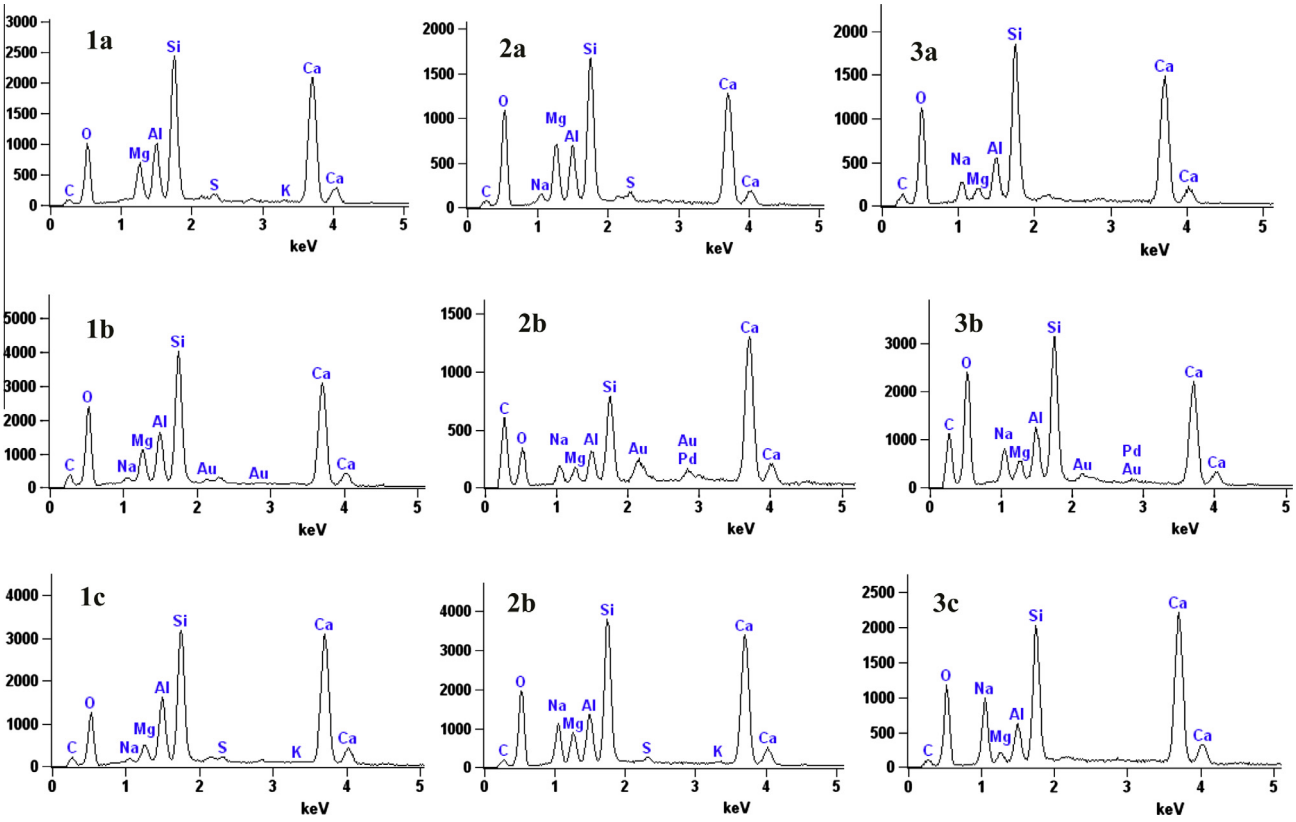

Fig. 14. Comparison of energy dispersive spectroscopy of slag activated by (a) 5 M, (b) 8 M and (c) 12 M NaOH solutions (1, 2 and 3 represent unreacted slag grain, inner product and outer product, respectively).

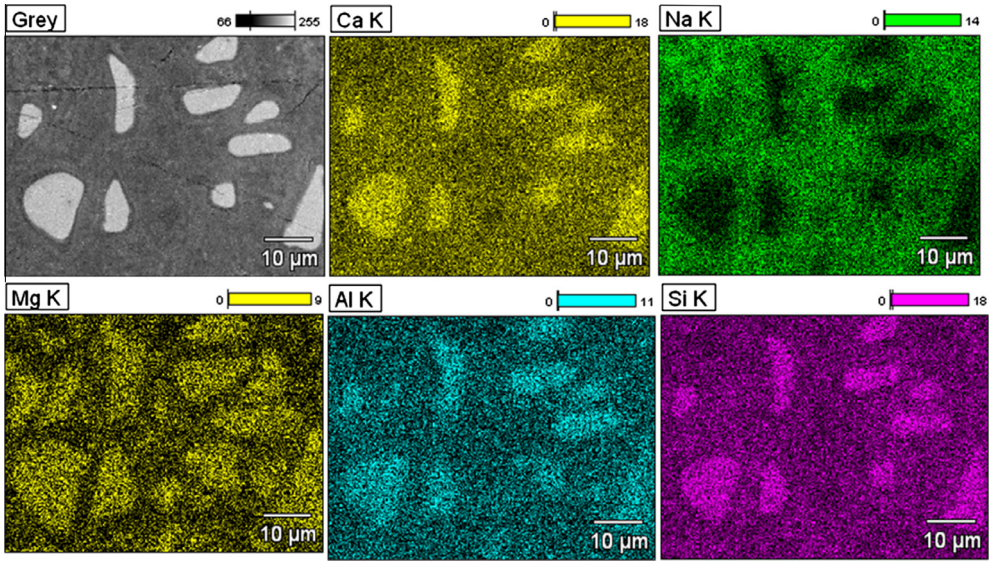

Fig. 15. Electron mapping of slag activated by 8 M NaOH after 28 days of hydration.

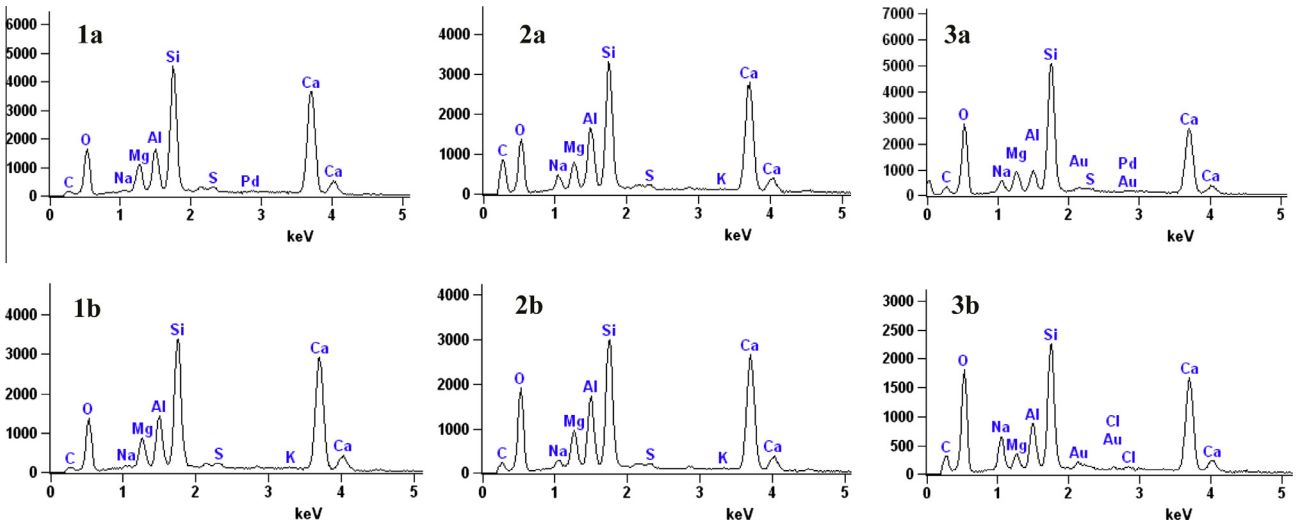

Fig. 16. Comparison of energy dispersive X-ray spectroscopy of slag activated by (a) 1.5 silica modulus and (b) 2.5 silica modulus SS solutions (1, 2 and 3 represent unreacted slag grain, inner product and outer product, respectively).

accelerators are provided. The hydration kinetics presented here are comparable to the results reported by Brough and Atkinson, [18] who identified the following stages: wetting, gelation of the activator, and bulk reaction of slag.

The microstructural development processes in NaOH and SS activated slag indicate two different hydration models. NaOH activated slag tends to form a thin layer of products around unreacted slag grains [11], which is spontaneous when the concentration of the NaOH activator is high. The thin layer formed acts as a physical barrier, slowing down the movement of ions to the slag grain surface and therefore the reaction with slag elements. However, because of the spontaneous reaction, well-formed microstructure is developed at the very early stage of hydration. Strength development and product formation are very fast in alkali activated slag compared to portland cement. Higher concentrations of Si and Na in the pore solution result in the fast precipitation of C–S–H at early stages of hydration [38]. Additionally, as NaOH molarity increases with constant solution/binder ratio, the free water content decreases. This results in a reduction of the mobility of ions, which is a likely explanation for the decreased rate of strength development in 12 M NaOH activated slag. The plateau in the cumulative heat evolution for this mixture suggests minimal product formation. Therefore, it can be seen that there is a direct relationship between the free water and the heat evolved from the hydration process.

Electron-mapping of some elements for the hydrated samples also showed the effect of the thin layer on the degree of diffusion of sodium into the unreacted grains and on the dissociation of calcium into the outer matrix [30,34]. The well-developed microstructure of NaOH activated slag reveals two product phases: inner product and outer product. The former is dense compared to the latter, which is more porous and prone to cracking [39–41]. SS-activated slag systems, on the other hand, allow adequate dissociation of ions from the slag particles into the pore solution which creates numerous nucleation sites. This allows the precipitation of new product from the solution. No immediate product formation is noted due to the prolonged dissociation and induction period. Given enough time, the strength developed for these types

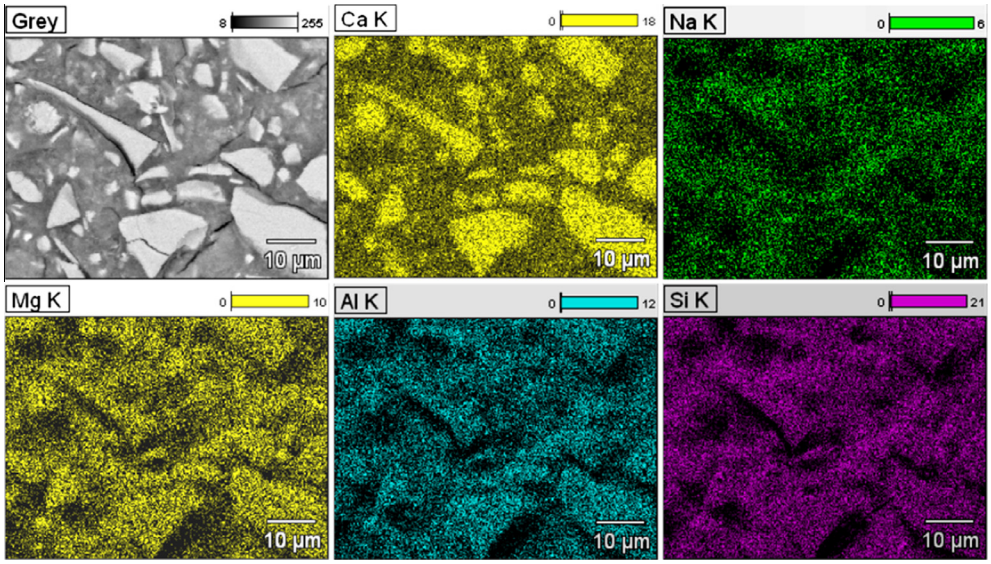

Fig. 17. Electron mapping of slag activated by SS (SiO_2/Na_2O = 1.5) after 28 days of hydration.

of activated systems is very impressive as a result of the sufficient dissociation of ions and the creation of plenty of nucleation sites [42].

The chemical composition of the products formed for both NaOH and SS activated slag did not show significant differences, regardless of the types and concentrations of alkali activators used. The main reaction products contain calcium and silicon, with traces of magnesium, aluminum, and sodium. This is in agreement with previous studies [11,19], although no traces of hydrotalcite were observed.

5. Conclusion

The influence of activator type and concentration on very early age reaction kinetics, microstructure, and composition of alkali activated slag paste were evaluated under ambient temperature curing conditions. In-situ isothermal calorimetric data shows the strong influence of activator type on the reaction kinetics. Activation of slag with sodium hydroxide initiates a rapid reaction process with a very short induction period at ambient temperature, whereas activation with sodium silicate results in a very long induction period. The concentration of each activating solution also has a very significant role, with higher dosage of the sodium hydroxide or higher silica modulus of sodium silicate resulting in higher heat evolution and reduced the duration of individual reaction stages. As a result, sodium hydroxide-activated systems develop an average of 30 MPa strength in the first day of hydration and do not show much difference as the hydration period is increased, while sodium silicate-activated systems develop strength more slowly, but can yield strengths as high as 70 MPa within 28 days.

Similarly, the microstructure in sodium hydroxide-activated slag is developed in the first one to two hours of curing, with very small progress after the first day of curing. The high alkalinity of the sodium hydroxide activator solution promotes the dissolution and product formation simultaneously, resulting in the formation of a reaction ring on the surfaces of the slag particles. The thickness of the reaction ring is inversely proportional to the concentration of the activating solution. The chemical composition of the reaction ring or the inner product is strongly affected by the concentration of sodium hydroxide activating solution. Sodium silicate activators, having additional silica and less sodium, allow for a higher degree of dissociation with many nucleation sites onto which products can grow. The microstructural development is slow with no reaction ring formation, and continues for several days, resulting in a stronger end product.

Acknowledgements

The authors gratefully acknowledge the financial support from the National Science Foundation (NSF) under CMMI Award no.1055641. Any opinions, findings, and conclusions or recommendations expressed in this article are those of the authors and do not necessarily reflect the views of the NSF.

References

[1] Lothenbach B, Scrivener K, Hooton RD. Supplementary cementitious materials. Cem Concr Res 2011;41(12):217–29.
[2] Wang SD, Pu XC, Scrivener KL, Pratt PL. Alkali-activated slag cement and concrete: a review of properties and problems. Adv Cem Res 1995;7(27):93–102.
[3] Monteiro P, Mehta K, Paulo JM. Concrete: Microstructure, properties and materials. McGraw-Hill; 2006.
[4] Chen K, Yang CH, Fang W, Ye JX, Pan Q, Yu ZD. Development of alkali activated slag cement based ecomaterial and its environmental coordination evaluation. Mater Sci Forum 2009;610:179–84.
[5] Fernando PT, Castro GJ, Jalali S. Alkali-activated binders: a review, Part 1. Historical background, terminology, reaction mechanisms and hydration products. Const Bldg Mater 2008;22:1305–14.
[6] Bijen J. Benefits of slag and flyash. Const Bldg Mater 1996;10:309–14.
[7] Roy DM. Alkali-activated cements: opportunities and challenges. Cem Concr Res 1999;29(2):249–54.
[8] Turner LK, Collins FG. Carbon dioxide equivalent (CO_2-e) emissions: a comparison between geopolymer and OPC cement concrete. Const Bldg Mater 2013;43:125–30.
[9] Deir E, Gebreziabiher BS, Peethamparan S. Influence of starting material on the early age hydration kinetics and the composition of binding gel in alkali activated binder systems. Cem Concr Compd 2014;48:108–17.
[10] Altan E, Erdogan ST. Alkali activation of a slag at ambient and elevated temperatures. Cem Concr Compd 2012;34(2):131–9.
[11] Haha MB, Saout GL, Winnefeld F, Lothenbach B. Influence of activator type on hydration kinetics, hydrate assemblage and microstructural development of alkali activated blast furnace slags. Cem Concr Res 2012;42(1):74–83.
[12] Fernandez-Jimenez A, Palomo JG, Puertas F. Alkali-activated slag mortars mechanical strength behavior. Cem Concr Res 1999;29(9):1313–21.
[13] Krizan D, Zovanovic B. Effects of dosage and modulus of water glass on early hydration of alkali–slag cements. Cem Concr Res 2002;32(8):1181–8.

[14] Sajedi F, Razak HA. The effect of chemical activators on early strength of ordinary Portland cement-slag mortars. Constr Bldg Mater 2010;24(10):1944–51.
[15] Shi C, Day RL. Some factors affecting early hydration of alkali-slag cements. Cem Concr Res 1996;26(3):439–41.
[16] Fernandez-Jimenez A, Puertas F. Alkali-activated slag cements: kinetic studies. Cem Concr Res 1997;27(3):359–68.
[17] Brough AR, Atkinson A. Sodium silicate-based, alkali-activated slag mortars Part I. Strength, hydration and microstructure. Cem Concr Res 2002;32(6):865–79.
[18] Sohn SD, Jennings HM, Mason TO. Hydration of alkali-activated ground granulated blast furnace slag. J Mater Sci 2000;35(1):249–57.
[19] Sohn SD, Jennings HM. Pore solution chemistry of alkali-activated ground granulated blast-furnace slag. Cem Concr Res 1999;29(2):159–70.
[20] Zivica V. Effects of type and dosage of alkaline activator and temperature on the properties of alkali-activated slag mixtures. Const Bldg Mater 2007;21(7):1463–9.
[21] Aydın S, Baradan B. Mechanical and microstructural properties of heat cured alkali-activated slag mortars. Mater Design 2012;35:374–83.
[22] Jansen D, Goetz-Neunhoeffer F, Lothenbach B, Neubauer J. The early hydration of Ordinary Portland Cement (OPC): an approach comparing measured heat flow with calculated heat flow from QXRD. Cem Concr Res 2012;42(1):134–8.
[23] Scrivener KL, Nonat A. Hydration of cementitious materials, present and future. Cem Concr Res 2011;41(7):651–65.
[24] Shi C, Day RL. A calorimetric study of early hydration of alkali-slag cement. Cem Concr Res 1995;25(6):1333–46.
[25] Lin F, Meyer C. Hydration kinetics modeling of Portland cement considering the effects of curing temperature and applied pressure. Cem Concr Res 2009;39(4):255–65.
[26] Bernal SA, Gutierrez RM, Provis JL, Rose V. Effect of silicate modulus and metakaolin incorporation on the carbonation of alkali silicate-activated slags. Cem Concr Res 2010;40(6):898–907.
[27] Diamond S. The patch microstructure in concrete: the effect of superplasticizer. Cem Concr Res 2006;36(4):776–9.
[28] Bakharev T, Sanjayan JG, Cheng YB. Effect of elevated temperature curing on properties of alkali-activated slag concrete. Cem Concr Res 1999;29(10):1619–25.
[29] Juilland P, Gallucci E, Flatt R, Scrivener K. Dissolution theory applied to the induction period in alite hydration. Cem Concr Res 2010;40(6):831–44.
[30] Chen W, Brouwers HJH. The hydration of slag, part 1: reaction models for alkali-activated slag. J Mater Sci 2007;42(2):428–43.
[31] Haha MB, Lothenbach B, Saout GL, Winnefeld F. Influence of slag chemistry on the hydration of alkali-activated blast-furnace slag — Part II: Effect of Al_2O_3. Cem Concr Res 2012;4(1):74–83.
[32] Bernal SA, Gutiérrez RMD, Pedraza AL, Provis JL, Rodriguez ED, Delvasto S. Effect of binder content on the performance of alkali-activated slag concretes. Cem Concr Res 2011;41(1):1–8.
[33] Atis CD, Bilim C, Çelik O, Karahan O. Influence of activator on the strength and drying shrinkage of alkali-activated slag mortar. Const Bldg Mater 2009;23(31):548–55.
[34] Phaira JW, Schulzb JC, Bertramc WK, Aldridge LP. Investigation of the microstructure of alkali-activated cements by neutron scattering. Cem Concr Res 2003;33(11):1811–24.
[35] Wang SD, Scrivener KL. Hydration products of alkali activated slag cement. Cem Concr Res 1995;25(3):561–71.
[36] Haha MB, Lothenbach B, Saout GL, Winnefeld F. Influence of slag chemistry on the hydration of alkali-activated blast-furnace slag — Part I: effect of MgO. Cem Concr Res 2011;41(9):955–63.
[37] Rothstein D, Thomas JJ, Christensen BJ, Jennings HM. Solubility behavior of Ca-, S-, Al-, and Si-bearing solid phases in Portland cement pore solutions as a function of hydration time. Cem Concr Res 2002;32(10):1663–71.
[38] Gruskovnjak A, Lothenbach B, Holzer L, Figi R, Winnefeld F. Hydration of alkali-activated slag: comparison with ordinary Portland cement. Adv Cem Res 2003;18(3):119–28.
[39] Richardson IG. The nature of C–S–H in hardened cement. Cem Concr Res 1999;29(8):1131–47.
[40] Puertas F, Fernández-Jiménez A, Blanco-Varela MT. Pore solution in alkali-activated slag cement pastes. Relation to the composition and structure of calcium silicate hydrate. Cem Concr Res 2004;34(1):139–48.
[41] Oh JE, Monteiro PJM, Jun SS, Choi S, Clark SM. The evolution of strength and crystalline phases for alkali-activated ground blast furnace slag and fly ash-based geopolymers. Cem Concr Res 2010;40(2):189–96.
[42] Hubler MH, Thomas JJ, Jennings HM. Influence of nucleation seeding on the hydration kinetics and compressive strength of alkali activated slag paste. Cem Concr Res 2011;41(8):842–6.